Research Article

Enhanced Channel Estimation for Double RIS-Aided MIMO Systems Using Coupled Tensor Decompositions

Gerald C. Nwalozie[1], André L. F. de Almeida[2], Martin Haardt[1]

1. Communications Research Laboratory (CRL), Technical University Ilmenau, Germany; 2. Wireless Telecom Research Group (GTEL), Universidade Federal do Ceará, Brazil

In this paper, we consider a double-RIS (D-RIS)-aided flat-fading MIMO system and propose an interference-free channel training and estimation protocol, where the two single-reflection links and the one double-reflection link are estimated separately. Specifically, by using the proposed training protocol, the signal measurements of a particular reflection link can be extracted interference-free from the measurements of the superposition of the three links. We show that some channels are associated with two different components of the received signal. Exploiting the common channels involved in the single and double reflection links while recasting the received signals as tensors, we formulate the coupled tensor-based least square Khatri-Rao factorization (C-KRAFT) algorithm which is a closed-form solution and an enhanced iterative solution with less restrictions on the identifiability constraints, the coupled-alternating least square (C-ALS) algorithm. The C-KRAFT and C-ALS based channel estimation schemes are used to obtain the channel matrices in both single and double reflection links. We show that the proposed coupled tensor decomposition-based channel estimation schemes offer more accurate channel estimates under less restrictive identifiability constraints compared to competing channel estimation methods. Simulation results are provided showing the effectiveness of the proposed algorithms.

Corresponding author: Gerald C. Nwalozie, gerald-chetachi.nwalozie@tu-ilmenau.de

1. Introduction

Reconfigurable intelligent surfaces (RIS) have been introduced recently as a key enabling technology for future wireless communication systems. An RIS is a 2D surface with a large number of inexpensive tunable elements, e.g., antennas or metamaterials[1][2]. Due to these potentials, RIS-aided communication systems have received significant attention in both academia and industry in the last few years. As a result, various RIS-aided communication systems have been studied, such as millimeter-wave (mmWave) communications, dynamic time division duplex (DTDD) based communication systems, cognitive radio, and unmanned aerial vehicle (UAV) communications[3][4][5][6][7].

However, in a passive RIS-aided communication system, where the RIS has no radio-frequency chains, channel estimation is a challenging task since it involves the estimation of multiple channels simultaneously. These include the direct

channels between the transmitter and each receiver, the channels between the RIS and the transmitter, and the channels between the RIS and each receiver[8]. Therefore, most existing references about RIS optimization techniques[3][4][5][6][7][8][9] assume that perfect channel state information (CSI) is available at the transceivers. However, this assumption is highly unlikely to hold in practice for an RIS-assisted system. Due to its passive nature, an RIS cannot send and receive pilot symbols and has no signal processing capability to estimate the channels. In this case, the channel estimation task should be carried out at the receiver using pilots reflected by the RISs.

Earlier works on RIS-aided systems have considered single RIS (S-RIS)-aided systems[10][11], where a single RIS is deployed between a user equipment (UE) and a base station (BS). Nonetheless, to further exploit the spatial diversity provided by multiple wireless links multi RIS-aided systems have started to receive more attention recently, where two or more RIS panels are deployed between a UE and a BS[12][13][14]. In[15][16], the authors showed that double RIS (D-RIS) aided systems have a much higher passive beamforming gain when compared to S-RIS aided systems, i.e., $\mathcal{O}(M_S^4)$ versus $\mathcal{O}(M_S^2)$, where M_S denotes the total number of reflective elements in both systems. Channel estimation in D-RIS systems, however, is more complicated than that in S-RIS systems, since the number of channels matrices to be estimated in D-RIS systems is larger compared to S-RIS based systems.

In[17][18], we have proposed alternating least squares (ALS)-based channel estimation methods for a D-RIS aided MIMO system by exploiting two tensor signal structures obtained from the channel training measurements. However, both methods consider simplified D-RIS aided MIMO systems, where only the double-reflection link from the BS to the UE across the two RISs is available. However, in order to achieve the maximum beamforming gain of a D-RIS-based system, not only the double-reflection link must be estimated, but also the other two single-reflection links. To this end, channel estimation methods for D-RIS aided systems considering both single-reflection and double-reflection links have been proposed recently, e.g.,[19][20][21][22]. In[20], the authors proposed a channel estimation protocol with two-time scales for active D-RIS-aided multi-user multiple-input single-output (MISO) systems, where the slowly time-varying channel is estimated by exploiting channel sparsity, and the fast time-varying channel is estimated using a measurement-augmentation estimate (MAE) compressed sensing strategy. This is based on estimating the fast time-varying channels at the BS using the estimates of the slowly time-varying channels. In[21], a multi-user single-input multiple-output (SIMO) system is considered where the channel estimation procedure is divided into three phases. In the first two phases, one of the two single-reflection links is estimated while turning off the other RIS. In the third phase, the double-reflection link is estimated after canceling the interference from the two single reflection links.

In this paper, we propose to exploit the benefits of coupled tensor decomposition techniques for channel estimation in a D-RIS-aided MIMO communication system, where the two single-reflection links and the one double-reflection link are estimated from three different tensors. In contrast to[23], our proposed methods exploit the fact that some of the channels are common to the double reflection link and the single reflection links. As a result, we exploit these structures and couple the resulting measurement signal tensors along the common dimension. We derive the decomposition structure of the resulting tensor, from which two new channel estimation algorithms are formulated. The adopted coupled tensor decomposition technique results in an improvement in the identifiability constraints and enhances the channel estimation accuracy in comparison to the state-of-the-art in[23].

In this way, the MIMO channels involved in a particular reflection link can be estimated from the extracted measurements using, e.g., the methods proposed in[10][18]. We show that the interference-free cascaded channel of each single-reflection link can be represented as a 3-way tensor that admits a canonical polyadic (CP) decomposition, while the double-reflection cascaded channel can be represented as a 4-way tensor admitting a nested-CP decomposition[18][24]. By coupling these received signal tensors, we derive, coupled tensor-based least square Khatri-Rao factorization (C-KRAFT) and coupled-ALS (C-ALS) based channel estimation schemes to obtain the channel matrices in both single and double reflection links. In the C-KRAFT scheme, which is a closed-form solution, the two coupled channels are estimated in parallel, while the other two channels are extracted from the coupled terms. Moreover, in the C-ALS scheme, which is an enhanced iterative solution with less restrictions in terms of the identifiability constraints, we estimate one of the channel matrices while assuming that the other channels are fixed. We also derive the identifiability conditions for the proposed channel estimation schemes, showing that the proposed coupled tensor decomposition-based algorithms offer less restrictive training settings compared to competing methods. Our proposed method is applicable not only to single-antenna UEs, but also to multi-antenna UEs which is different from the work in[21]. Simulation results are provided showing the effectiveness of the proposed channel training protocol.

Notation:

The transpose, the conjugate transpose (Hermitian), the Moore–Penrose inverse, the Kronecker product, and the Khatri-Rao product are denoted as $\mathbf{X}^{\mathsf{T}}$, $\mathbf{X}^{\mathsf{H}}$, $\mathbf{X}^{+}$, $\otimes$, $\diamond$, respectively. Moreover, $\mathrm{diag}\{\mathbf{x}\}$ forms a diagonal matrix $\mathbf{X}$ by putting the entries of the input vector $\mathbf{x}$ in its main diagonal, $\mathrm{vec}\{\mathbf{X}\}$ forms a vector by staking the columns of $\mathbf{X}$ over each other, $\mathrm{unvec}\{\mathbf{x}\}$ is the inverse of the vec operator. Furthermore, $\|\mathbf{a}\|_2$ represents the 2-norm and $\|\mathbf{A}\|_{\mathrm{F}}$ denotes the Frobenius norm. The expression $\mathcal{X} \times_n \mathbf{A}$ gives the n-mode product between a tensor $\mathcal{X} \in \mathbb{C}^{I_1 \times \cdots I_n \cdots I_R}$ and a matrix $\mathbf{A} \in \mathbb{C}^{I_n \times J_n}$ that produces the resulting tensor $\mathcal{Y} \in \mathbb{C}^{I_1 \times \cdots J_n \cdots I_R}$. Additionally, $\mathbf{Y}_{(n)}$ represents the n-mode unfolding of the tensor $\mathbf{Y}$.

2. System Model

We consider a D-RIS-aided MIMO communication system as shown in Fig. 1, where two RISs, i.e., RIS 1 and RIS 2, are deployed to assist the communication between a UE with M_{UE} antennas and a BS with M_{BS} antennas. As depicted in Fig. 1, we assume that RIS 1 with M_{S1} reflecting elements is placed closer to the BS while RIS 2 with M_{S2} reflecting elements is placed closer to the UE. Similarly to[21], we assume that the direct channel between the BS and the UE is neglectable due to severe signal blockage and pathloss.

Let $\mathbf{G}_1 \in \mathbb{C}^{M_{\mathrm{S1}} \times M_{\mathrm{UE}}}$, $\mathbf{G}_2 \in \mathbb{C}^{M_{\mathrm{S2}} \times M_{\mathrm{UE}}}$, $\mathbf{H}_1 \in \mathbb{C}^{M_{\mathrm{BS}} \times M_{\mathrm{S1}}}$, $\mathbf{H}_2 \in \mathbb{C}^{M_{\mathrm{BS}} \times M_{\mathrm{S2}}}$, $\mathbf{T} \in \mathbb{C}^{M_{\mathrm{S2}} \times M_{\mathrm{S1}}}$ denote the UE-to-RIS 1, UE-to-RIS 2, RIS 1-to-BS, RIS 2-to-BS, and RIS 1-to-RIS 2 channels, respectively. Then, the received signal at the (i, j, k)th transmission time can be expressed as

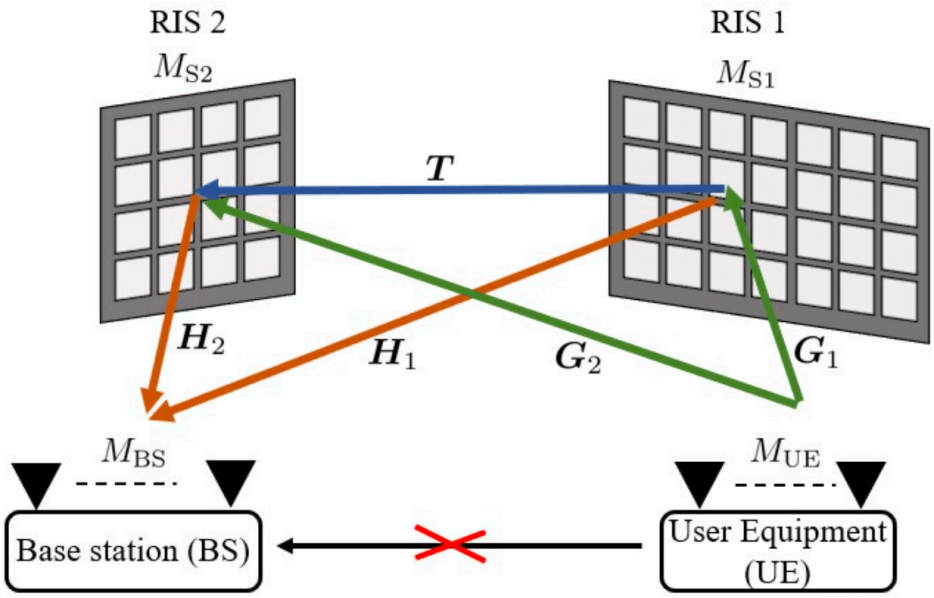

Figure 1. A D-RIS-aided MIMO communication system.

$$\overline{\mathbf{y}}_{i,j,k} = \mathbf{H}_2 \text{diag}\{\boldsymbol{\theta}_{2,j}\}\mathbf{T}\text{diag}\{\boldsymbol{\theta}_{1,i}\}\mathbf{G}_1\mathbf{x}_k + \mathbf{H}_1\text{diag}\{\boldsymbol{\theta}_{1,i}\}\mathbf{G}_1\mathbf{x}_k + \mathbf{H}_2\text{diag}\{\boldsymbol{\theta}_{2,j}\}\mathbf{G}_2\mathbf{x}_k + \overline{\mathbf{n}}_{i,j,k} \in \mathbb{C}^{M_{\text{BS}}}, \tag{1}$$

where $\mathbf{x}_k \in \mathbb{C}^{M_{\text{UE}}}$ is the kth training vector at UE with $\|\mathbf{x}_k\|_2^2 = 1, k \in \{1, \cdots, K\}$, $\boldsymbol{\theta}_{1,i} \in \mathbb{C}^{M_{\text{S1}}}$ is the ith training beam of RIS 1 with $|[\boldsymbol{\theta}_{1,i}]_{[m]}| = \frac{1}{\sqrt{M_{\text{S1}}}}$, $i \in \{1, \cdots, I\}$, $\boldsymbol{\theta}_{2,j} \in \mathbb{C}^{M_{\text{S2}}}$ is the jth training beam of RIS 2 with $|[\boldsymbol{\theta}_{2,j}]_{[n]}| = \frac{1}{\sqrt{M_{\text{S2}}}}, \forall n$, $j \in \{1, \cdots, J\}$, and $\overline{\mathbf{n}}_{i,j,k} \in \mathbb{C}^{M_{\text{BS}}}$ is the additive white Guassian noise (AWGN) with variance σ_n^2. Note that the received signal at the BS in (1) is comprised of three parts, **Component 1** denotes the single-reflection component via RIS 1 (second term), **Component 2** is the single-reflection component via RIS 2 (third term), and **Component 3** comprises the double-reflection component via RIS 1 and RIS 2 (the first term).

Let $\mathbf{X} = [\mathbf{x}_1, \cdots, \mathbf{x}_K] \in \mathbb{C}^{M_{\text{UE}} \times K}$ denote the training pilot at the transmitter during one frame. Then, by collecting the received signals $\{\overline{\mathbf{y}}_{i,j,k}\}_{k=1}^K$ at the BS next to each other, we obtain

$$\overline{\mathbf{Y}}_{i,j} = \mathbf{H}_2 \text{diag}\{\boldsymbol{\theta}_{2,j}\}\mathbf{T}\text{diag}\{\boldsymbol{\theta}_{1,i}\}\mathbf{G}_1\mathbf{X} + \mathbf{H}_1\text{diag}\{\boldsymbol{\theta}_{1,i}\}\mathbf{G}_1\mathbf{X} + \mathbf{H}_2\text{diag}\{\boldsymbol{\theta}_{2,j}\}\mathbf{G}_2\mathbf{X} + \overline{\mathbf{N}}_{i,j} \in \mathbb{C}^{M_{\text{BS}} \times K}, \tag{2}$$

where $\overline{\mathbf{N}}_{i,j}$ is defined similarly to $\overline{\mathbf{Y}}_{i,j}$. We assume that $\mathbf{X}$ is designed with orthonormal rows, i.e., $\mathbf{X}\mathbf{X}^{\text{H}} = \mathbf{I}_{M_{\text{UE}}}$, which implies that $K \geq M_{\text{UE}}$. Then, the right filtered measurement matrix $\mathbf{Y}_{i,j} = \overline{\mathbf{Y}}_{i,j}\mathbf{X}^{\text{H}}$ can be expressed as

$$\mathbf{Y}_{i,j} = \mathbf{H}_2 \text{diag}\{\boldsymbol{\theta}_{2,j}\}\mathbf{T}\text{diag}\{\boldsymbol{\theta}_{1,i}\}\mathbf{G}_1 + \mathbf{H}_1\text{diag}\{\boldsymbol{\theta}_{1,i}\}\mathbf{G}_1 + \mathbf{H}_2\text{diag}\{\boldsymbol{\theta}_{2,j}\}\mathbf{G}_2 + \mathbf{N}_{i,j} \in \mathbb{C}^{M_{\text{BS}} \times M_{\text{UE}}}, \tag{3}$$

where $\mathbf{N}_{i,j} = \overline{\mathbf{N}}_{i,j}\mathbf{X}^{\text{H}}$.

doi.org/10.32388/V5XHXK

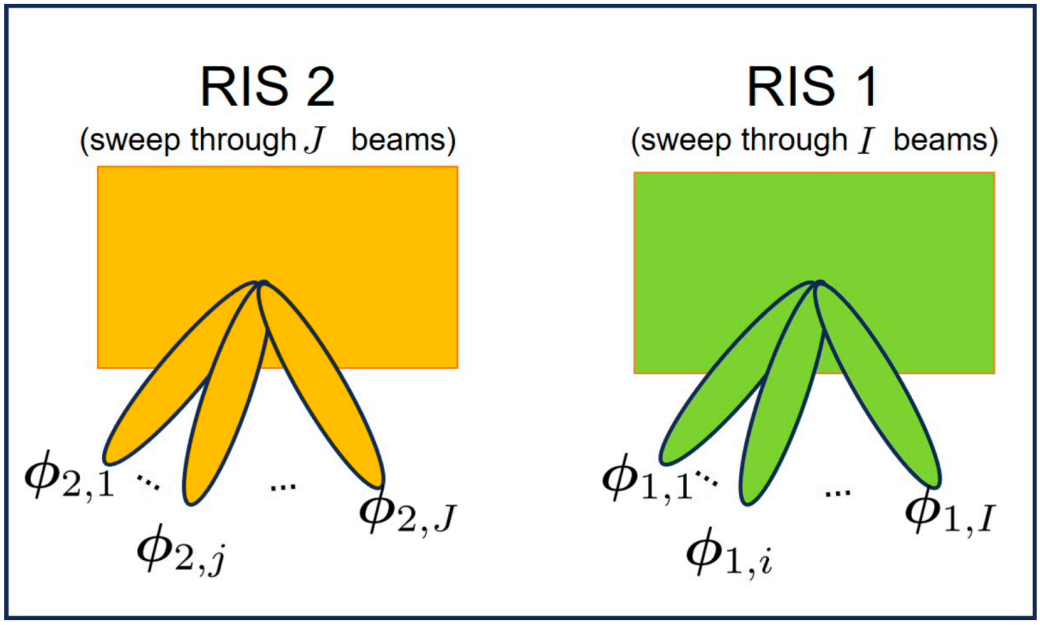

Figure 2. The training procedure.

The training beams of the RISs $\boldsymbol{\theta}_{1,i}, \forall i$, and $\boldsymbol{\theta}_{2,j}, \forall j$, can have two states: State 0 and State 1. In State 0, the training beams are designed as

$$\boldsymbol{\theta}^0_{\mu,q} = [e^{j\theta_1}, \ldots, e^{j\theta_{M_{\mathrm{S}\mu}}}]^{\mathsf{T}} = \boldsymbol{\theta}_{\mu,q} \in \mathbb{C}^{M_{\mathrm{S}\mu}}, \tag{4}$$

and in State 1, the training beams are designed as

$$\boldsymbol{\theta}^1_{\mu,q} = [e^{j(\theta_1+\pi)}, \ldots, e^{j(\theta_{M_{\mathrm{S}\mu}}+\pi)}]^{\mathsf{T}} = -\boldsymbol{\theta}_{\mu,q} \in \mathbb{C}^{M_{\mathrm{S}\mu}}, \tag{5}$$

with $\mu \in \{1, 2\}$ and $q \in \{i, j\}$. This training protocol is an extension of the training protocol in[25] for S-RIS aided systems to the case of D-RIS aided systems. To estimate the channels, we perform a channel training procedure for the RISs as illustrated in Fig. 2. Specifically, for every ith training beam of RIS 1, i.e., $\phi_{1,i} \in \mathbb{C}^{M_{\mathrm{S}1}}$, $i \in \{1, \ldots, I\}$, we sweep through the J training beams of RIS 2, i.e., $\{\phi_{2,1}, \ldots, \phi_{2,J}\}$, where $\phi_{2,j} \in \mathbb{C}^{M_{\mathrm{S}2}}, \forall j$. At this time, the training beams of both RISs are in State 0. Therefore, the obtained measurement matrices during Stage 1 are given as

$$Y^{0,0}_{i,j} = H_2 \mathrm{diag}\{\theta^0_{2,j}\} T \mathrm{diag}\{\theta^0_{1,i}\} G_1 + H_1 \mathrm{diag}\{\theta^0_{1,i}\} G_1 + H_2 \mathrm{diag}\{\theta^0_{2,j}\} G_2 + N^{0,0}_{i,j} \in \mathbb{C}^{M_{\mathrm{BS}} \times M_{\mathrm{UE}}}. \tag{6}$$

Here we use all the combinations of $i, \forall i = 1, \cdots, I$ and $j, \forall j = 1, \cdots, J$.

Channel training procedure for Component 1:

To estimate G_1 and H_1 in Component 1, as shown in Fig. 3 (b), we switch the state of a selected training beam of RIS 2 from State 0 to State 1, i.e., $\theta^1_{2,j}$, while we sweep again through the I training beams of RIS 1, i.e., $\{\theta^0_{1,1}, \ldots, \theta^0_{1,I}\}$. Thus, the obtained measurement matrices during Stage 2 are

$$Y^{0,1}_{i,j} = H_2 \mathrm{diag}\{\theta^1_{2,j}\} T \mathrm{diag}\{\theta^0_{1,i}\} G_1 + H_1 \mathrm{diag}\{\theta^0_{1,i}\} G_1 + H_2 \mathrm{diag}\{\theta^1_{2,j}\} G_2 + N^{0,1}_{i,j} \in \mathbb{C}^{M_{\mathrm{BS}} \times M_{\mathrm{UE}}} \tag{7}$$

doi.org/10.32388/V5XHXK

Therefore, by combining (6) and (7) and recalling that $\theta_{2,j}^{1} = -\theta_{2,j}^{0}$, we obtain the measurement matrices $Y_{i,j}^{(1)}$ as

$$Y_{i,j}^{(1)} \triangleq Y_{i,j}^{0,0} + Y_{i,j}^{0,1} = 2H_1 \text{diag}\{\theta_{1,i}^{0}\} G_1 + N_{i,j}^{(1)}, \tag{8}$$

where $N_{i,j}^{(1)} = N_{i,j}^{0,0} + N_{i,j}^{0,1}$. Note that (8) depends only on the training vectors of the RIS 1, i.e., $\{\theta_{1,1}^{0}, \ldots, \theta_{1,I}^{0}\}$.

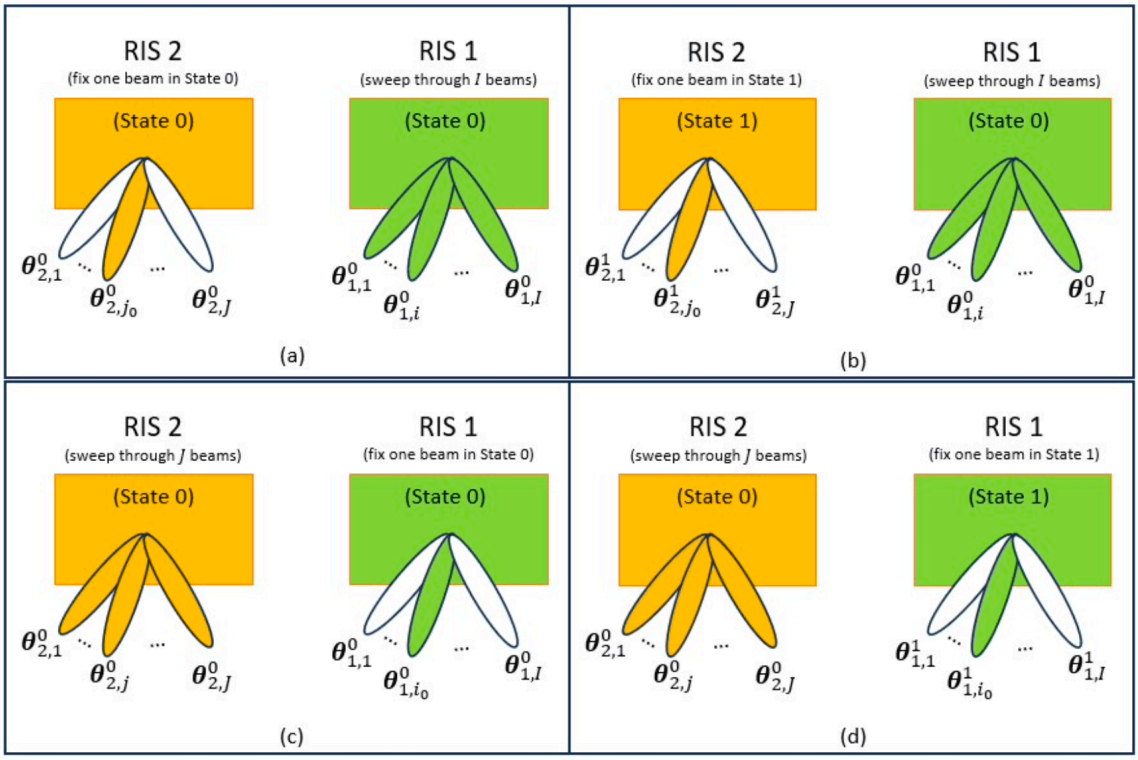

Figure 3. The training procedures to estimate the channels in Component 1 ((a) and (b)) and the channels in Component 2 ((c) and (d)).

Channel training procedure for Component 2:

To estimate G_2 and H_2 in Component 2, we perform another channel training as illustrated in Fig. 3 (b), we switch the state of a selected training beam of RIS 1 from State 0 to State 1, i.e., $\theta_{1,i}^{1}$, while we sweep again through the J beams of RIS 2, i.e., $\{\theta_{2,1}^{0}, \ldots, \theta_{2,J}^{0}\}$ and the obtained measurement matrix is written as

$$Y_{i,j}^{1,0} = H_2 \text{diag}\{\theta_{2,j}^{0}\} T \text{diag}\{\theta_{1,i}^{1}\} G_1 + H_1 \text{diag}\{\theta_{1,i}^{1}\} G_1 + H_2 \text{diag}\{\theta_{2,j}^{0}\} G_2 + N_{i,j}^{1,0} \in \mathbb{C}^{M_{\text{BS}} \times M_{\text{UE}}}. \tag{9}$$

Similarly, combining (6) and (9), we obtain the measurement matrix $Y_{i,j}^{(2)}$ as

$$\mathbf{Y}_{i,j}^{(2)} \triangleq \mathbf{Y}_{i,j}^{0,0} + \mathbf{Y}_{i,j}^{1,0} = 2\mathbf{H}_2 \text{diag}\{\theta_{2,j}^{0}\} \mathbf{G}_2 + \mathbf{N}_{i,j}^{(2)}, \tag{10}$$

where $\mathbf{N}_{i,j}^{(2)} = \mathbf{N}_{i,j}^{0,0} + \mathbf{N}_{i,j}^{1,0}$. Note that (10) is as a result of the fact that $\theta_{1,i}^{1} = -\theta_{1,i}^{0}$.

doi.org/10.32388/V5XHXK

Channel training procedure for Component 3:

To estimate the channel matrix $\mathbf{T} \in \mathbb{C}^{M_{S2} \times M_{S1}}$ in Component 3, we combine the measurement matrices in (7) and (9) as follows

$$\begin{aligned} \mathbf{Y}_{i,j}^{(3)} &\triangleq -\mathbf{Y}_{i,j}^{1,0} - \mathbf{Y}_{i,j}^{0,1} \\ &= 2\mathbf{H}_2 \text{diag}\{\theta_{2,j}\}\mathbf{T}\text{diag}\{\theta_{1,i}\}\mathbf{G}_1 + \mathbf{N}_{i,j}^{(3)}. \end{aligned} \tag{11}$$

This procedure will avoid the error propagation in the approach adopted in [23] for the estimation of this double reflection link.

The estimates of these channels can be readily obtained by using the methods in [23]. However, the approach in [23] has identifiability constraints which in turn affect the estimation accuracy. Moreover, from Fig. 1, we observe that the channels $\mathbf{G}_1$ and $\mathbf{H}_2$ are each associated with two different components of the received signal at the BS. Therefore, in the following, we propose to exploit these structures and the inherent benefitsof coupled tensor decompositions to improve the identifiability and the resulting estimation accuracy.

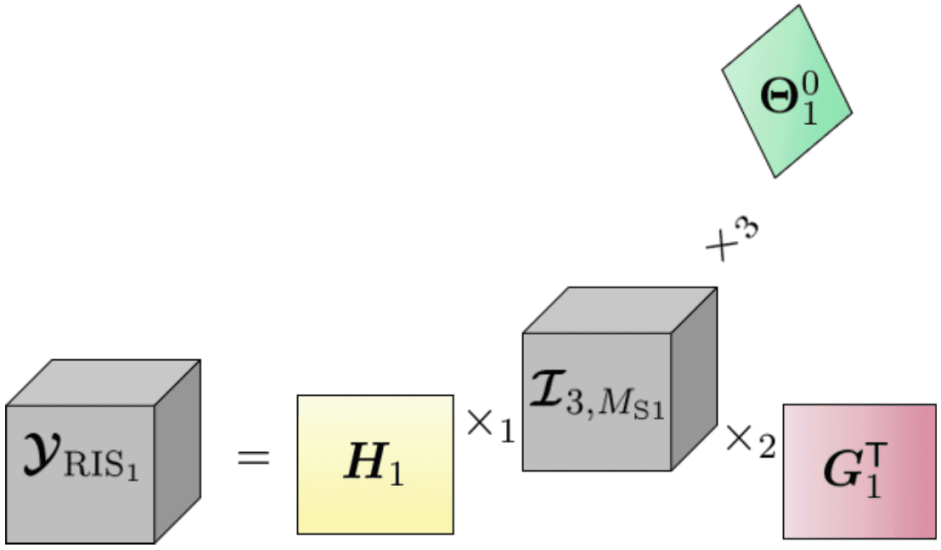

Figure 4. Graphical representation of the 3-way tensor $\mathcal{Y}_{\text{RIS}_1}$

3. Tensor Signal Modeling

In this section, we note that the received measurement matrices for the different components in Section 2 can be recast as a 3-way tensor following CP and nested-CP models. Therefore, by relying on these received signals we are able to jointly estimate all the channels using coupled tensor decomposition algorithms.

To begin, we note that specifically in [10], it is shown that the measurement matrix in (8) that only depends on the training beams of RIS 1 can be arranged into a 3-way tensor $\mathcal{Y}_{\text{RIS}_1} \in \mathbb{C}^{M_{\text{BS}} \times M_{\text{UE}} \times I}$ admitting a CP decomposition as

$$\mathcal{Y}_{\text{RIS}_1} = \mathcal{I}_{3,M_{S1}} \times_1 \mathbf{H}_1 \times_2 \mathbf{G}_1^{\mathsf{T}} \times_3 \boldsymbol{\Theta}_1^0 + \mathcal{N}_{\text{RIS}_1}, \tag{12}$$

where $\boldsymbol{\Theta}_1^0 = \left[\theta_{1,1}^0, \cdots, \theta_{1,I}^0\right]^{\mathsf{T}} \in \mathbb{C}^{I \times M_{\mathrm{S1}}}$. The tensor $\mathcal{Y}_{\mathrm{RIS}_1}$, as shown in Fig. 4, has the following n-mode unfoldings, $n \in \{1, 2, 3\}$,

$$\left[\mathcal{Y}_{\mathrm{RIS}_1}\right]_{(1)} = \mathbf{H}_1 \left(\boldsymbol{\Theta}_1^0 \diamond \mathbf{G}_1^{\mathsf{T}}\right)^{\mathsf{T}} + \left[\mathcal{N}_{\mathrm{RIS}_1}\right]_{(1)} \in \mathbb{C}^{M_{\mathrm{BS}} \times I M_{\mathrm{UE}}} \tag{13}$$

$$\left[\mathcal{Y}_{\mathrm{RIS}_1}\right]_{(2)} = \mathbf{G}_1^{\mathsf{T}} \left(\boldsymbol{\Theta}_1^0 \diamond \mathbf{H}_1\right)^{\mathsf{T}} + \left[\mathcal{N}_{\mathrm{RIS}_1}\right]_{(2)} \in \mathbb{C}^{M_{\mathrm{UE}} \times I M_{\mathrm{BS}}} \tag{14}$$

$$\left[\mathcal{Y}_{\mathrm{RIS}_1}\right]_{(3)} = \boldsymbol{\Theta}_1^0 \left(\mathbf{G}_1^{\mathsf{T}} \diamond \mathbf{H}_1\right)^{\mathsf{T}} + \left[\mathcal{N}_{\mathrm{RIS}_1}\right]_{(3)} \in \mathbb{C}^{I \times M_{\mathrm{BS}} M_{\mathrm{UE}}} \tag{15}$$

In the same way, we observe that the measurement matrix in (10) can be written as a 3-way tensor $\mathcal{Y}_{\mathrm{RIS}_2} \in \mathbb{C}^{M_{\mathrm{BS}} \times M_{\mathrm{UE}} \times J}$ admitting a CP decomposition (see Fig. 5) as

$$\mathcal{Y}_{\mathrm{RIS}_2} = \mathcal{I}_{3,M_{\mathrm{S2}}} \times_1 \mathbf{H}_2 \times_2 \mathbf{G}_2^{\mathsf{T}} \times_3 \boldsymbol{\Theta}_2^0 + \mathcal{N}_{\mathrm{RIS}_2}, \tag{16}$$

where $\boldsymbol{\Theta}_2^0 = \left[\theta_{2,1}^0, \cdots, \theta_{2,J}^0\right]^{\mathsf{T}} \in \mathbb{C}^{J \times M_{\mathrm{S2}}}$ and the n-mode unfoldings, $n \in \{1, 2, 3\}$, can be written as

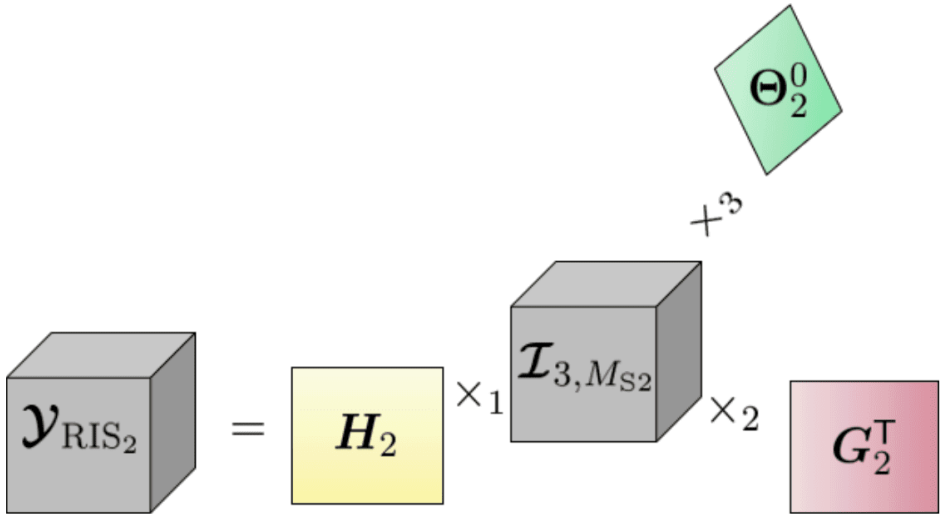

Figure 5. Graphical representation of the 3-way tensor $\mathcal{Y}_{\mathrm{RIS}_2}$

$$\left[\mathcal{Y}_{\mathrm{RIS}_2}\right]_{(1)} = \mathbf{H}_2 \left(\boldsymbol{\Theta}_2^0 \circ \mathbf{G}_2^{\mathsf{T}}\right)^{\mathsf{T}} + \left[\mathcal{N}_{\mathrm{RIS}_2}\right]_{(1)} \in \mathbb{C}^{M_{\mathrm{BS}} \times J M_{\mathrm{UE}}} \tag{17}$$

$$\left[\mathcal{Y}_{\mathrm{RIS}_2}\right]_{(2)} = \mathbf{G}_2^{\mathsf{T}} \left(\boldsymbol{\Theta}_2^0 \circ \mathbf{H}_2\right)^{\mathsf{T}} + \left[\mathcal{N}_{\mathrm{RIS}_2}\right]_{(2)} \in \mathbb{C}^{M_{\mathrm{UE}} \times J M_{\mathrm{BS}}} \tag{18}$$

$$\left[\mathcal{Y}_{\mathrm{RIS}_2}\right]_{(3)} = \boldsymbol{\Theta}_2^0 \left(\mathbf{G}_2^{\mathsf{T}} \circ \mathbf{H}_2\right)^{\mathsf{T}} + \left[\mathcal{N}_{\mathrm{RIS}_2}\right]_{(3)} \in \mathbb{C}^{J \times M_{\mathrm{BS}} M_{\mathrm{UE}}} \tag{19}$$

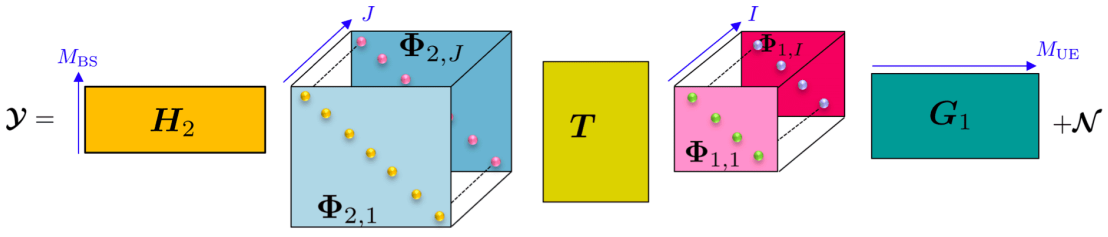

Figure 6. Graphical representation of the 4-way tensor $\mathcal{Y}$

Furthermore, we have shown in our previous work [18] that the measurement matrices $\mathbf{Y}_{i,j}^{(3)}$ in (11) can be arranged into a 3-way tensor $\mathcal{Y}$ admitting a nested-CP decomposition as shown in Fig. 6. Moreover, let $\mathcal{W} \in \mathbb{C}^{M_{\mathrm{UE}} \times I \times M_{\mathrm{S2}}}$ and $\mathcal{U} \in \mathbb{C}^{M_{\mathrm{BS}} \times J \times M_{\mathrm{S1}}}$ denote two 3-way CP tensors as

$$\mathcal{W} = \mathcal{I}_{3,M_{\mathrm{S1}}} \times_1 \mathbf{G}_1^{\mathsf{T}} \times_2 \mathbf{\Theta}_1^0 \times_3 \mathbf{T} \in \mathbb{C}^{M_{\mathrm{UE}} \times I \times M_{\mathrm{S2}}}, \tag{20}$$
$$\mathcal{U} = \mathcal{I}_{3,M_{\mathrm{S2}}} \times_1 \mathbf{H}_2 \times_2 \mathbf{\Theta}_2^0 \times_3 \mathbf{T}^{\mathsf{T}} \in \mathbb{C}^{M_{\mathrm{BS}} \times J \times M_{\mathrm{S1}}}. \tag{21}$$

Therefore, the tensor $\mathcal{Y}$ can be written in either of the following two forms depending on the choice of the mode combination of $\mathcal{Y}$ with associated CP models in (20) and (21), [26]

$$\mathcal{Y}^{(1)} = \mathcal{I}_{3,M_{\mathrm{S2}}} \times_1 \mathbf{H}_2 \times_2 [\mathcal{W}]_{(3)}^{\mathsf{T}} \times_3 \mathbf{\Theta}_2^0 \in \mathbb{C}^{M_{\mathrm{BS}} \times IM_{\mathrm{UE}} \times J}$$
$$\mathcal{Y}^{(2)} = \mathcal{I}_{3,M_{\mathrm{S1}}} \times_1 [\mathcal{U}]_{(3)}^{\mathsf{T}} \times_2 \mathbf{G}_1^{\mathsf{T}} \times_3 \mathbf{\Theta}_1^0 \in \mathbb{C}^{M_{\mathrm{BS}} J \times M_{\mathrm{UE}} \times I},$$

where $[\mathcal{W}]_{(3)}^{\mathsf{T}} = \left(\mathbf{\Theta}_1^0 \circ \mathbf{G}_1^{\mathsf{T}}\right) \mathbf{T}^{\mathsf{T}} \in \mathbb{C}^{IM_{\mathrm{UE}} \times M_{\mathrm{S2}}}$ and $[\mathcal{U}]_{(3)}^{\mathsf{T}} = \left(\mathbf{\Theta}_2^0 \circ \mathbf{H}_2\right) \mathbf{T} \in \mathbb{C}^{JM_{\mathrm{BS}} \times M_{\mathrm{S1}}}$ denotes the transposed 3-mode unfoldings of $\mathcal{W}$ and $\mathcal{U}$, respectively. Therefore, as shown in [18] the n-mode unfoldings of the tensor $\mathcal{Y}^{(1)}$, $n \in \{1,2,3\}$ can be written as

$$\left[\mathcal{Y}^{(1)}\right]_{(1)} = \mathbf{H}_2 \left(\mathbf{\Theta}_2^0 \circ [\mathcal{W}]_{(3)}^{\mathsf{T}}\right)^{\mathsf{T}} + \left[\mathcal{N}^{(1)}\right]_{(1)} \in \mathbb{C}^{M_{\mathrm{BS}} \times JIM_{\mathrm{UE}}} \tag{22}$$
$$\left[\mathcal{Y}^{(1)}\right]_{(2)} = [\mathcal{W}]_{(3)}^{\mathsf{T}} \left(\mathbf{\Theta}_2^0 \circ \mathbf{H}_2\right)^{\mathsf{T}} + \left[\mathcal{N}^{(1)}\right]_{(2)} \in \mathbb{C}^{IM_{\mathrm{UE}} \times JM_{\mathrm{BS}}} \tag{23}$$
$$\left[\mathcal{Y}^{(1)}\right]_{(3)} = \mathbf{\Theta}_2^0 \left([\mathcal{W}]_{(3)}^{\mathsf{T}} \circ \mathbf{H}_2\right)^{\mathsf{T}} + \left[\mathcal{N}^{(1)}\right]_{(3)} \in \mathbb{C}^{J \times IM_{\mathrm{UE}} M_{\mathrm{BS}}}. \tag{24}$$

In the same way, the n-mode unfoldings of the tensor $\mathcal{Y}^{(2)}$ $n \in \{1,2,3\}$, can be written as

$$\left[\mathcal{Y}^{(2)}\right]_{(1)} = [\mathcal{U}]_{(3)}^{\mathsf{T}} \left(\mathbf{\Theta}_1^0 \circ \mathbf{G}_1^{\mathsf{T}}\right)^{\mathsf{T}} + \left[\mathcal{N}^{(2)}\right]_{(1)} \in \mathbb{C}^{JM_{\mathrm{BS}} \times IM_{\mathrm{UE}}} \tag{25}$$
$$\left[\mathcal{Y}^{(2)}\right]_{(2)} = \mathbf{G}_1^{\mathsf{T}} \left(\mathbf{\Theta}_1^0 \circ [\mathcal{U}]_{(3)}^{\mathsf{T}}\right)^{\mathsf{T}} + \left[\mathcal{N}^{(2)}\right]_{(2)} \in \mathbb{C}^{M_{\mathrm{UE}} \times IJM_{\mathrm{BS}}} \tag{26}$$
$$\left[\mathcal{Y}^{(2)}\right]_{(3)} = \mathbf{\Theta}_1^0 \left(\mathbf{G}_1^{\mathsf{T}} \circ [\mathcal{U}]_{(3)}^{\mathsf{T}}\right)^{\mathsf{T}} + \left[\mathcal{N}^{(2)}\right]_{(3)} \in \mathbb{C}^{J \times IM_{\mathrm{UE}} M_{\mathrm{BS}}} \tag{27}$$

Here, we observe that there are similarities in the structure of the 2-mode unfoldings of $\mathcal{Y}^{(2)}$ and $\mathcal{Y}_{\mathrm{RIS}_1}$ given in (14) and (26), respectively, and the 1-mode unfoldings $\mathcal{Y}_{\mathrm{RIS}_2}$ and $\mathcal{Y}^{(1)}$ given in (17) and (22), respectively. In the following, we propose to exploit these structure similarities and adopt coupled tensor decomposition techniques to estimate $\mathbf{G}_1$,$\mathbf{H}_1$, $\mathbf{G}_2$, $\mathbf{H}_2$, and $\mathbf{T}$ in order to improve the identifiability constraints and enhance the channel estimation accuracy.

3.1. Coupled tensor-based channel estimation

In this section, relying on the tensor signal models developed in the previous section, we formulate the proposed coupled tensor-based channel estimation algorithm by combining the received signal tensors at the BS, i.e., $\mathcal{Y}^{(1)}$, $\mathcal{Y}^{(2)}$, $\mathcal{Y}_{\mathrm{RIS}_1}$, and $\mathcal{Y}_{\mathrm{RIS}_2}$.

Estimate channels in Component 1: From (14) and (26) we discover that the channel matrix $\mathbf{G}_1$ is common to the 2-mode unfoldings of $\mathcal{Y}^{(2)}$ and $\mathcal{Y}_{\mathrm{RIS}_1}$. Therefore, we denote $\tilde{\mathbf{Y}}_1$ as a matrix that stacks the two 2-mode unfoldings of $\mathcal{Y}^{(2)}$ and $\mathcal{Y}_{\mathrm{RIS}_1}$ along the second dimension, i.e., $\tilde{\mathbf{Y}}_1 = \begin{bmatrix} \left[\mathcal{Y}_{\mathrm{RIS}_1}\right]_{(2)} & \left[\mathcal{Y}^{(2)}\right]_{(2)} \end{bmatrix} \in \mathbb{C}^{M_{\mathrm{UE}} \times I(J+1)M_{\mathrm{BS}}}$ as

$$\begin{aligned} \tilde{\mathbf{Y}}_1 &= \begin{bmatrix} \mathbf{G}_1^T \left(\mathbf{\Theta}_1^0 \circ \mathbf{H}_1\right)^T & \mathbf{G}_1^T \left(\mathbf{\Theta}_1^0 \circ [\mathcal{U}]_{(3)}^T\right)^T \end{bmatrix}, \\ &= \mathbf{G}_1^T \begin{bmatrix} \left(\mathbf{\Theta}_1^0 \circ \mathbf{H}_1\right)^T & \left(\mathbf{\Theta}_1^0 \circ [\mathcal{U}]_{(3)}^T\right)^T \end{bmatrix}. \end{aligned} \tag{28}$$

We can further express (28) as (see Appendix A for the proof)

$$\mathbf{Y}_1 = \tilde{\mathbf{Y}}_1 \mathbf{P}_1 = \mathbf{G}_1^T \left(\mathbf{\Theta}_1^0 \circ \mathbf{\Sigma}_1\right)^T, \tag{29}$$

where $\mathbf{\Sigma}_1 = \begin{bmatrix} \mathbf{H}_1 \\ [\mathcal{U}]_{(3)}^T \end{bmatrix}$ and $\mathbf{P}_1$ is a permutation matrix. It should be noted that (29) can be written as a tensor $\mathcal{Y}_1 \in \mathbb{C}^{M_{\text{UE}} \times (J+1)M_{\text{BS}} \times I}$ which admits a CP decomposition with a coupled nested-CP model as

$$\mathcal{Y}_1 = \mathcal{I}_{3,M_{\text{S1}}} \times_1 \mathbf{G}_1^T \times_2 \mathbf{\Sigma}_1 \times_3 \mathbf{\Theta}_1^0 + \mathcal{N}_1. \tag{30}$$

Therefore, we can write the n-mode unfoldings of $\mathcal{Y}_1$, i.e., $n \in \{1,2,3\}$, as

$$[\mathcal{Y}_1]_{(1)} = \mathbf{G}_1^T \left(\mathbf{\Theta}_1^0 \circ \mathbf{\Sigma}_1\right)^T + [\mathcal{N}_1]_{(1)} \in \mathbb{C}^{M_{\text{UE}} \times I(J+1)M_{\text{BS}}} \tag{31}$$

$$[\mathcal{Y}_1]_{(2)} = \mathbf{\Sigma}_1 \left(\mathbf{\Theta}_1^0 \circ \mathbf{G}_1^T\right)^T + [\mathcal{N}_1]_{(2)} \in \mathbb{C}^{(J+1)M_{\text{BS}} \times I M_{\text{UE}}} \tag{32}$$

$$[\mathcal{Y}_1]_{(3)} = \mathbf{\Theta}_1^0 \left(\mathbf{\Sigma}_1 \circ \mathbf{G}_1^T\right)^T + [\mathcal{N}_1]_{(3)} \in \mathbb{C}^{I \times (J+1)M_{\text{BS}} M_{\text{UE}}}. \tag{33}$$

Estimate channels in Component 2: To proceed, we note that the channel matrix $\mathbf{H}_2$ is common to the 1-mode unfoldings of $\mathcal{Y}^{(1)}$ and $\mathcal{Y}_{\text{RIS}_2}$ given in (22) and (17), respectively. Similarly, we define $\tilde{\mathbf{Y}}_2$ as a matrix that stacks the 1-mode unfoldings of $\mathcal{Y}$ and $\mathcal{Y}_{\text{RIS}_2}$ along the second dimension, i.e., $\tilde{\mathbf{Y}}_2 = \begin{bmatrix} [\mathcal{Y}_{\text{RIS}_2}]_{(1)} & \left[\mathcal{Y}^{(1)}\right]_{(1)} \end{bmatrix} \in \mathbb{C}^{M_{\text{BS}} \times J(I+1)M_{\text{UE}}}$ as

$$\begin{aligned} \tilde{\mathbf{Y}}_2 &= \begin{bmatrix} \mathbf{H}_2 \left(\mathbf{\Theta}_2^0 \circ \mathbf{G}_2^{\mathsf{T}}\right)^{\mathsf{T}} & \mathbf{H}_2 \left(\mathbf{\Theta}_2^0 \circ [\mathbf{W}]_{(3)}^{\mathsf{T}}\right)^{\mathsf{T}} \end{bmatrix}, \\ &= \mathbf{H}_2 \begin{bmatrix} \left(\mathbf{\Theta}_2^0 \circ \mathbf{G}_2^{\mathsf{T}}\right)^{\mathsf{T}} & \left(\mathbf{\Theta}_2^0 \circ [\mathbf{W}]_{(3)}^{\mathsf{T}}\right)^{\mathsf{T}} \end{bmatrix}. \end{aligned} \tag{34}$$

Then, we can further express (34) in a similar manner as (29) as

$$\mathbf{Y}_2 = \tilde{\mathbf{Y}}_2 \mathbf{P}_2 = \mathbf{H}_2 \left(\mathbf{\Theta}_2^0 \circ \mathbf{\Sigma}_2\right)^{\mathsf{T}}, \tag{35}$$

where $\mathbf{\Sigma}_2 = \begin{bmatrix} \mathbf{G}_2^{\mathsf{T}} \\ [\mathbf{W}]_{(3)}^{\mathsf{T}} \end{bmatrix}$ and $\mathbf{P}_2$ is a permutation matrix. The measurement matrix in (35) can also be written as a tensor $\mathbf{Y}_2 \in \mathbb{C}^{M_{\text{BS}} \times (I+1)M_{\text{UE}} \times J}$ which admits a CP decomposition with a coupled nested-CP structure as

$$\mathbf{Y}_2 = \mathbf{I}_{3,M_{\text{S2}}} \times_1 \mathbf{H}_2 \times_2 \mathbf{\Sigma}_2 \times_3 \mathbf{\Theta}_2^0 + \mathbf{N}_2, \tag{36}$$

and its n-mode unfoldings, i.e., $n \in \{1,2,3\}$, are given as

$$[\mathbf{Y}_2]_{(1)} = \mathbf{H}_2 \left(\mathbf{\Theta}_2^0 \circ \mathbf{\Sigma}_2\right)^{\mathsf{T}} + [\mathbf{N}_2]_{(1)} \in \mathbb{C}^{M_{\text{BS}} \times J(I+1)M_{\text{UE}}} \tag{37}$$

$$[\mathbf{Y}_2]_{(2)} = \mathbf{\Sigma}_2 \left(\mathbf{\Theta}_2^0 \circ \mathbf{H}_2\right)^{\mathsf{T}} + [\mathbf{N}_2]_{(2)} \in \mathbb{C}^{(I+1)M_{\text{UE}} \times J M_{\text{BS}}} \tag{38}$$

$$[\mathbf{Y}_2]_{(3)} = \mathbf{\Theta}_2^0 (\mathbf{\Sigma}_2 \circ \mathbf{H}_2)^{\mathsf{T}} + [\mathbf{N}_2]_{(3)} \in \mathbb{C}^{J \times (I+1)M_{\text{UE}} J M_{\text{BS}}} \tag{39}$$

Estimate channel in Component 3: The channel $\mathbf{T} \in \mathbb{C}^{M_{\text{S2}} \times M_{\text{S1}}}$ in Component 3 can easily be estimated by adopting the approach in [24]. We note that the measurement matrix in (11) is a generalized unfolding of a 4-way tensor admitting a nested-CP decomposition, which can be utilized to estimate the channel matrix $\mathbf{T}$, i.e., $\mathbf{Y}_{i,j}^{(3)} = [\mathbf{Y}_3]_{([1,2],[3,4])}$. Therefore, the generalized unfolding [27] is given as

$$[\mathbf{Y}_3]_{([1,2],[3,4])} = \left(\mathbf{\Theta}_2^0 \circ \mathbf{H}_2\right) \mathbf{T} \left(\mathbf{\Theta}_1^0 \circ \mathbf{G}_1^{\mathsf{T}}\right)^{\mathsf{T}} \in \mathbb{C}^{J M_{\text{BS}} \times I M_{\text{UE}}}, \tag{40}$$

where the each factor $(\mathbf{\Theta}_2^0 \circ \mathbf{H}_2)$ and $(\mathbf{\Theta}_1^0 \circ \mathbf{G}_1^{\mathsf{T}})$ results from the combination of the first two modes of the $\mathbf{U}$ and $\mathbf{W}$ tensor, respectively, whereas the middle factor $\mathbf{T}$ is the common factor to the CP decompositions of these tensors. In

the following, we propose two solutions for estimating $\mathbf{G}_1$,$\mathbf{H}_1$, $\mathbf{G}_2$, $\mathbf{H}_2$, and $\mathbf{T}$ by exploiting the above tensor structures.

3.1.1. Coupled-Khatri-Rao Factorization (C-KRAFT)

Assume that the training matrices $\mathbf{\Theta}_1^0$ and $\mathbf{\Theta}_2^0$ are designed with orthonormal columns, i.e., $\mathbf{\Theta}_1^{0\mathsf{H}}\mathbf{\Theta}_1^0 = \mathbf{I}_I$ and $\mathbf{\Theta}_2^{0\mathsf{H}}\mathbf{\Theta}_2^0 = \mathbf{I}_J$. Then, the left-filtered 3-mode unfoldings of $\mathcal{Y}_1$ in (33) and $\mathcal{Y}_2$ in (39) are given as

$$\left[\overline{\mathcal{Y}}_1\right]_{(3)} = \mathbf{\Theta}_1^{0\mathsf{H}}[\mathcal{Y}_1]_{(3)} = \left(\mathbf{\Sigma}_1 \diamond \mathbf{G}_1^{\mathsf{T}}\right)^{\mathsf{T}} + \left[\overline{\mathcal{N}}_1\right]_{(3)}, \tag{41}$$

$$\left[\overline{\mathcal{Y}}_2\right]_{(3)} = \mathbf{\Theta}_2^{0\mathsf{H}}[\mathcal{Y}_2]_{(3)} = \left(\mathbf{\Sigma}_2 \diamond \mathbf{H}_2\right)^{\mathsf{T}} + \left[\overline{\mathcal{N}}_2\right]_{(3)}, \tag{42}$$

where $\left[\overline{\mathcal{N}}_1\right]_{(3)} = \mathbf{\Theta}_1^{0\mathsf{H}}[\mathcal{N}_1]_{(3)}$ and $\left[\overline{\mathcal{N}}_2\right]_{(3)} = \mathbf{\Theta}_2^{0\mathsf{H}}[\mathcal{N}_2]_{(3)}$ are the left-filtered noise matrices.

Therefore, the estimates of $\mathbf{G}_1$, $\mathbf{\Sigma}_1$, $\mathbf{H}_2$, and $\mathbf{\Sigma}_2$ can be obtained as a solution to following problems, using $\left[\overline{\mathcal{Y}}_1\right]_{(3)}$ and $\left[\overline{\mathcal{Y}}_2\right]_{(3)}$, respectively,

$$(\hat{\mathbf{G}}_1, \hat{\mathbf{\Sigma}}_1) = \underset{\mathbf{G}_1, \mathbf{\Sigma}_1}{\operatorname{argmin}} \left\| \left[\overline{\mathcal{Y}}_1\right]_{(3)}^{\mathsf{T}} - \left(\mathbf{\Sigma}_1 \diamond \mathbf{G}_1^{\mathsf{T}}\right) \right\|_{\mathrm{F}}^2, \tag{43}$$

$$(\hat{\mathbf{H}}_2, \hat{\mathbf{\Sigma}}_2) = \underset{\mathbf{H}_2, \mathbf{\Sigma}_2}{\operatorname{argmin}} \left\| \left[\overline{\mathcal{Y}}_2\right]_{(3)}^{\mathsf{T}} - \left(\mathbf{\Sigma}_2 \diamond \mathbf{H}_2\right) \right\|_{\mathrm{F}}^2. \tag{44}$$

Closed-form solutions to the above problems are easily obtained by using the least squares Khatrio-Rao Factorization (KRF) technique[28][29][30]. Then, $\hat{\mathbf{H}}_1$ and $\hat{\mathbf{G}}_2$ can be obtained from $\hat{\mathbf{\Sigma}}_1$ and $\hat{\mathbf{\Sigma}}_2$ by extracting the first M_{BS} rows of $\hat{\mathbf{\Sigma}}_1$ and first M_{UE} rows of $\hat{\mathbf{\Sigma}}_2$, respectively as, $\hat{\mathbf{H}}_1 = \left[\hat{\mathbf{\Sigma}}_1\right]_{[1:M_{\mathrm{BS}},:]}$ and $\hat{\mathbf{G}}_2 = \left[\hat{\mathbf{\Sigma}}_2\right]_{[1:M_{\mathrm{UE}},:]}$. Then, to obtain the estimate of $\mathbf{T}$ we apply bilinear filtering to (40) as

$$\hat{\mathbf{T}} = \left[\left(\mathbf{\Theta}_1^0 \diamond \hat{\mathbf{G}}_1^{\mathsf{T}} \right)^{+} [\mathcal{Y}_3]_{(1,2),(3,4)}^{\mathsf{T}} \left(\mathbf{\Theta}_2^0 \diamond \hat{\mathbf{H}}_2 \right)^{\mathsf{T}} \right]^{+}. \tag{45}$$

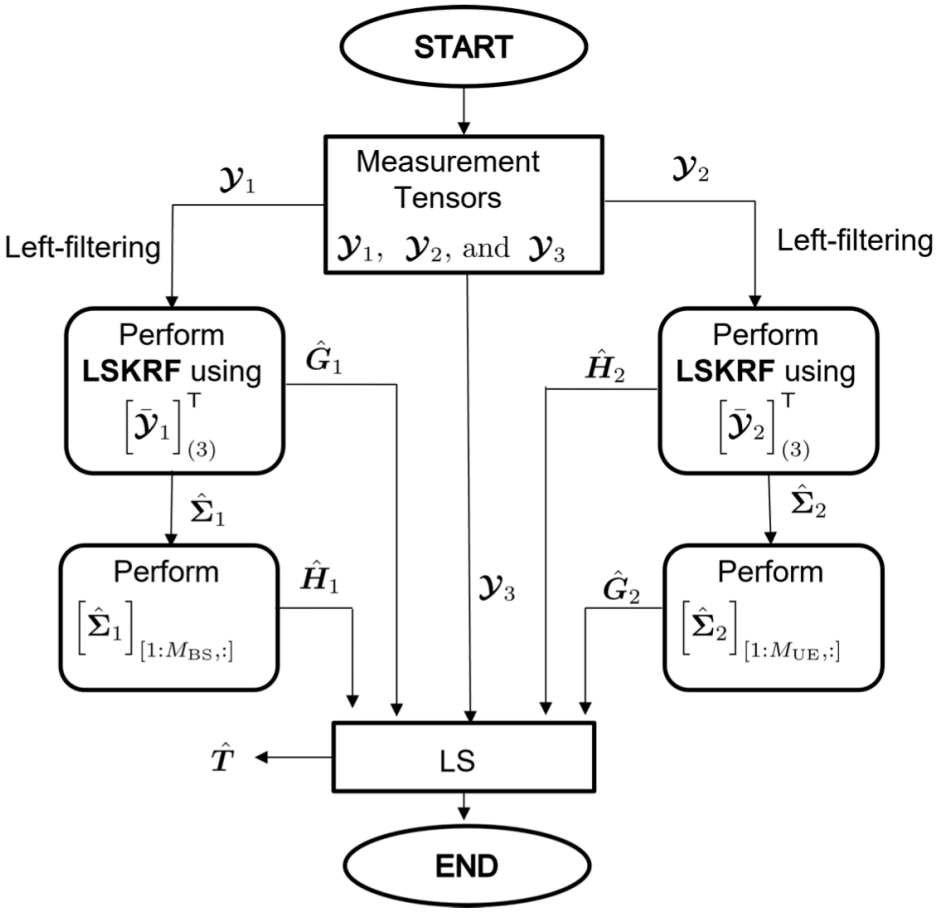

Figure 7. Graphical representation of the C-KRAFT algorithm

The proposed closed-form C-KRAFT-based channel estimation for double-RIS aided MIMO systems is summarized in Fig. 7 and Algorithm 1. The C-KRAFT-based method can be computationally less expensive, however, it may not give a better estimation result. Motivated by the need to improve the accuracy of the channel estimation, in the following, we propose a coupled tensor-based ALS method for the estimation of the channels.

doi.org/10.32388/V5XHXK

Input: Measurement tensors $\mathcal{Y}_1, \mathcal{Y}_2$
1: Get $\hat{\mathbf{G}}_1$ and $\hat{\mathbf{\Sigma}}_1$ as a solution to (43) using Algorithm 1[29].
2: Get $\hat{\mathbf{H}}_2$ and $\hat{\mathbf{\Sigma}}_2$ as a solution to (44) using Algorithm 1[29].
3: Get $\hat{\mathbf{H}}_1$ as $\hat{\mathbf{H}}_1 = \left[\hat{\mathbf{\Sigma}}_1\right]_{[1:M_{\mathrm{BS}},:]}$
4: Get $\hat{\mathbf{G}}_2$ as $\hat{\mathbf{G}}_2 = \left[\hat{\mathbf{\Sigma}}_2\right]_{[1:M_{\mathrm{UE}},:]}$
5: Get $\hat{\mathbf{T}}$ as in (45) using the given $\hat{\mathbf{G}}_1$ and $\hat{\mathbf{H}}_2$
Output: $\hat{\mathbf{G}}_1$, $\hat{\mathbf{H}}_1$,$\hat{\mathbf{H}}_2$, $\hat{\mathbf{G}}_2$, and $\hat{\mathbf{T}}$

Algorithm 1. C-KRAFT-based CE for DRIS Systems

3.1.2. Coupled-Alternating Least Squares (C-ALS)

In this section, to improve the estimation accuracy we propose a coupled tensor-based ALS (C-ALS) algorithm which minimizes the data fitting error with respect to one of the channels, with the other channels being fixed. To begin, we note that from the 1-mode unfolding of the coupled tensor $\mathcal{Y}_1$ in (30) the common channel $\mathbf{G}_1$ can be estimated using least square (LS) as

$$\hat{\mathbf{G}}_1 = \left\{ [\mathcal{Y}_1]_{(1)} \left[\left(\mathbf{\Theta}_1^0 \diamond \mathbf{\Sigma}_1 \right)^{\mathsf{T}} \right]^{+} \right\}^{\mathsf{T}}. \tag{46}$$

Then, the estimate of the remaining channel in component 1 is obtained by exploiting (13) since the channel is not coupled to any other links. The LS estimate of $\mathbf{H}_1$ is obtained as

$$\hat{\mathbf{H}}_1 = \left[\mathcal{Y}_{\mathrm{RIS}_1}\right]_{(1)} \left[\left(\mathbf{\Theta}_1^0 \diamond \mathbf{G}_1^{\mathsf{T}} \right)^{\mathsf{T}} \right]^{+}. \tag{47}$$

Next, we consider the estimate of the other common channel $\mathbf{H}_2$ by exploiting the 1-mode unfoldingof the coupled tensor $\mathcal{Y}_2$ in (37). As a result, the LS estimate of $\mathbf{H}_2$ can be obtained as

$$\hat{\mathbf{H}}_2 = [\mathcal{Y}_2]_{(1)} \left[\left(\mathbf{\Sigma}_2 \diamond \mathbf{\Theta}_2^0 \right)^{\mathsf{T}} \right]^{+}. \tag{48}$$

The LS estimate of $\mathbf{G}_2$ is obtained from (18) as

$$\hat{\mathbf{G}}_2 = \left\{ \left[\mathcal{Y}_{\mathrm{RIS}_2}\right]_{(2)} \left[\left(\mathbf{\Theta}_2^0 \diamond \mathbf{H}_2 \right)^{\mathsf{T}} \right]^{+} \right\}^{\mathsf{T}}. \tag{49}$$

Finally, we update $\hat{\mathbf{T}}$ by using (45). Therefore, the coupled tensor-based ALS channel estimation for a double-RIS aided MIMO system is summarized in Algorithm 2, which is guaranteed to converge monotonically to a local optimum point[31].

Algorithm 2 C-ALS-based CE for DRIS Systems

Input: Measurement tensors $\boldsymbol{\mathcal{Y}}_{\mathrm{RIS}_1}$, $\boldsymbol{\mathcal{Y}}_{\mathrm{RIS}_2}$, $\boldsymbol{\mathcal{Y}}$, and select $t_{\max}$

Initialize: $\hat{\boldsymbol{H}}_1^{(0)}$, $\hat{\boldsymbol{H}}_2^{(0)}$, $\hat{\boldsymbol{G}}_2^{(0)}$, $\hat{\boldsymbol{T}}^{(0)}$, e.g., as solution of C-KRAFT algorithm .

for $t = 1$ to $t_{\max}$ **do**

$$\hat{\boldsymbol{G}}_1^{(t)} = \left\{ \left[\boldsymbol{\mathcal{Y}}_1 \right]_{(1)} \left[\left(\boldsymbol{\Theta}_1^0 \diamond \boldsymbol{\Sigma}_1^{(t-1)} \right)^{\mathsf{T}} \right]^{+} \right\}^{\mathsf{T}}$$

$$\hat{\boldsymbol{H}}_1^{(t)} = \left[\boldsymbol{\mathcal{Y}}_{\mathrm{RIS}_1} \right]_{(1)} \left[\left(\boldsymbol{\Theta}_1^0 \diamond (\hat{\boldsymbol{G}}_1^{(t)})^{\mathsf{T}} \right)^{\mathsf{T}} \right]^{+}$$

$$\hat{\boldsymbol{H}}_2^{(t)} = \left[\boldsymbol{\mathcal{Y}}_2 \right]_{(1)} \left[\left(\boldsymbol{\Theta}_2^0 \diamond \boldsymbol{\Sigma}_2^{(t-1)} \right)^{\mathsf{T}} \right]^{+}$$

$$\hat{\boldsymbol{G}}_2^{(t)} = \left\{ \left[\boldsymbol{\mathcal{Y}}_{\mathrm{RIS}_2} \right]_{(2)} \left[\left(\boldsymbol{\Theta}_2^0 \diamond \boldsymbol{H}_2^{(t)} \right)^{\mathsf{T}} \right]^{+} \right\}^{\mathsf{T}}$$

$$\hat{\boldsymbol{T}}^{(t)} = \left[(\boldsymbol{\Theta}_1^0 \diamond (\hat{\boldsymbol{G}}_1^{(t)})^{\mathsf{T}}) \right]^{+} \left[\boldsymbol{\mathcal{Y}}_3 \right]_{([1,2],[3,4])}^{\mathsf{T}} \left[(\boldsymbol{\Theta}_2^0 \diamond \hat{\boldsymbol{H}}_2^{(t)})^{\mathsf{T}} \right]^{+}$$

end for

Output: $\hat{\boldsymbol{G}}_1$, $\hat{\boldsymbol{H}}_1$,$\hat{\boldsymbol{H}}_2$, $\hat{\boldsymbol{G}}_2$, and $\hat{\boldsymbol{T}}$

3.2. Identifiablity conditions

As far as the estimation of the single reflection links and the double reflection link are concerned, the study of identifiability conditions of the associated tensor models is relevant. Indeed, these conditions indicate the required system setups that lead to a unique estimation of the involved channel matrices. To this end, in the following, we derive a set of conditions involving system parameters such as the required number of training frames, and the number of receive and transmit antennas for accurate channel estimation.

3.2.1. C-KRAFT based method

In this section, we provide the identifiability conditions associated with the estimation of the D-RIS channels by using the C-KRAFT method in Algorithm 1. The C-KRAFT based algorithm in LS sense requires that $K \geq M_{\mathrm{UE}}$, $I \geq M_{\mathrm{S1}}$ and $J \geq M_{\mathrm{S2}}$ for accurate estimation of $\mathbf{G}_1$ and $\boldsymbol{\Sigma}_1$ and $\mathbf{G}_2$ and $\boldsymbol{\Sigma}_2$, respectively.

3.2.2. C-ALS based method

In this section, we give the identifiablity conditions associated with the estimation of the D-RIS channels by using the C-ALS method in Algorithm 2.

Component 1: The LS estimation of $\mathbf{G}_1$ and $\mathbf{H}_1$ requires that each of the following matrices $(\boldsymbol{\Theta}_1^0 \diamond \boldsymbol{\Sigma}_1)^{\mathsf{T}} \in \mathbb{C}^{M_{\mathrm{S1}} \times I(J+1)M_{\mathrm{BS}}}$ in (46) and $\left(\boldsymbol{\Theta}_1^0 \diamond \mathbf{G}_1^{\mathsf{T}}\right)^{\mathsf{T}} \in \mathbb{C}^{IM_{\mathrm{UE}} \times M_{\mathrm{S1}}}$ in (47) has a unique right Moore-Penrose pseudo-inverse, i.e., full row-rank. This implies that I needs to satisfy the condition of $I \geq \max\left\{ \lceil \frac{M_{\mathrm{S1}}}{M_{\mathrm{UE}}} \rceil, \lceil \frac{M_{\mathrm{S1}}}{(J+1)M_{\mathrm{BS}}} \rceil \right\}$ and $K \geq M_{\mathrm{UE}}$ to have accurate channel estimates in the LS sense. This demonstrates a significant gain of $(J+1)$ in the identifiability condition by using this coupled tensor approach as compared to the state-of-the-art in[23].

Component 2:

By investigating (48) and (49), we note that to have accurate channel estimates of $\mathbf{G}_2$ and $\mathbf{H}_2$ in LS sense J needs to satisfy the condition of $J \geq \max\left\{\lceil\frac{M_{\mathrm{S2}}}{(I+1)M_{\mathrm{UE}}}\rceil, \lceil\frac{M_{\mathrm{S2}}}{M_{\mathrm{BS}}}\rceil\right\}$ and $K \geq M_{\mathrm{UE}}$ to have accurate channel estimates in the LS sense. In the same way, due to the coupled tensor approach adopted in this work, we obtain an improvement in the identifiability condition for the channels in components 2 in comparison to the work in[23] where J needs to satisfy the condition $J \geq \max\left\{\lceil\frac{M_{\mathrm{S2}}}{M_{\mathrm{UE}}}\rceil, \lceil\frac{M_{\mathrm{S2}}}{M_{\mathrm{BS}}}\rceil, 2\right\}$ to have accurate channel estimates in the LS sense.

Component 3:

Note that the training procedure shown in Fig. 2 implies that IJK training overhead is required when estimating the channel $\mathbf{T}$ in Component 3. By investigating (45), I and J need to satisfy the conditions $I \geq \lceil\frac{M_{\mathrm{S1}}}{M_{\mathrm{UE}}}\rceil$ and $J \geq \lceil\frac{M_{\mathrm{S2}}}{M_{\mathrm{BS}}}\rceil$, respectively, to have an accurate channel estimate, assuming that $\mathrm{rank}\{\mathbf{\Theta}_1^0\} = I$ and $\mathrm{rank}\{\mathbf{\Theta}_2^0\} = J$.

We have summarized the identifiability conditions and the computational cost of the considered algorithms in Table 1, where $t_{\max}$ is the number of maximum iterations for the ALS-based schemes. We note that from the measurement tensors in (30) and (36), both I and J need to be greater or equal to 2, i.e., $I \geq 2$ and $J \geq 2$.

Method	Identifiablity	Computational Cost
C-KRAFT	$K \geq M_{\mathrm{UE}}, I \geq M_{\mathrm{S1}}, J \geq M_{\mathrm{S2}}$	$\mathcal{O}(2M_{\mathrm{S1}}^2 + 2M_{\mathrm{S2}}^2)$
C-ALS	$I \geq \max\{\lceil\frac{M_{\mathrm{S1}}}{M_{\mathrm{UE}}}\rceil, \lceil\frac{M_{\mathrm{S1}}}{(J+1)M_{\mathrm{BS}}}\rceil\}, J \geq \max\{\lceil\frac{M_{\mathrm{S2}}}{(I+1)M_{\mathrm{UE}}}\rceil, \lceil\frac{M_{\mathrm{S2}}}{M_{\mathrm{BS}}}\rceil\}, K \geq M_{\mathrm{UE}}$	$\mathcal{O}(t_{\max}(2M_{\mathrm{S1}}^3 + 2M_{\mathrm{S2}}^3))$
ALS[23]	$J \geq \max\{\lceil\frac{M_{\mathrm{S2}}}{M_{\mathrm{UE}}}\rceil, \lceil\frac{M_{\mathrm{S2}}}{M_{\mathrm{BS}}}\rceil, 2\}, I \geq \max\{\lceil\frac{M_{\mathrm{S1}}}{M_{\mathrm{UE}}}\rceil, \lceil\frac{M_{\mathrm{S1}}}{M_{\mathrm{BS}}}\rceil, 2\}, K \geq M_{\mathrm{UE}}$	$\mathcal{O}(t_{\max}(2M_{\mathrm{S1}}^3 + 2M_{\mathrm{S2}}^3 + (M_{\mathrm{S1}}M_{\mathrm{S2}})^3))$

Table 1. Identifiablity and Computational Cost

Ambiguities:

The ambiguities of the estimated channels in each of the components can be determined using a similar approach as in[17]. It was shown in[17] that the estimated channels are unique up to scalar ambiguities per column. For example, these ambiguities between the estimated and the true channels in component 3 can be written as

$$\hat{\mathbf{T}} \approx \mathbf{\Delta}_2^{-1}\mathbf{T}\mathbf{\Delta}_1^{-1}, \quad \hat{\mathbf{H}}_2 \approx \mathbf{H}_2\mathbf{\Delta}_2, \quad \hat{\mathbf{G}}_1 \approx \mathbf{\Delta}_1\mathbf{G}_1$$

where $\mathbf{\Lambda}_1$ and $\mathbf{\Lambda}_2$ are diagonal matrices holding the scaling ambiguities. However, these ambiguities have no impact on the reconstructed estimate of the effective end-to-end channel $\mathbf{H}_2\mathbf{T}\mathbf{G}_1$ as their effects disappear. Note that, due to the knowledge of the RIS reflection matrices $\mathbf{\Theta}_1^0$ and $\mathbf{\Theta}_2^0$ at the receiver, the permutation ambiguities do not exist[10]. The ambiguities in the estimated channels in the other components can be determined by following a similar approach.

4. Simulation Results

We assume that the entries of $\mathbf{G}_1$, $\mathbf{G}_2$, $\mathbf{H}_1$, $\mathbf{H}_2$, and $\mathbf{T}$ are independent and identically distributed zero-mean circularly-symmetric complex Gaussian random variables. We show results in terms of the normalized-mean-squared-error (NMSE) of the cascaded channels as

$$\text{NMSE} = \frac{\mathbb{E}\left\{\left\|\hat{\mathbf{P}}_x - \mathbf{P}_x\right\|_{\text{F}}^2\right\}}{\mathbb{E}\left\{\left\|\mathbf{P}_x\right\|_{\text{F}}^2\right\}}, \tag{50}$$

where $\mathbf{P}_x$ is the effective cascaded channel for component x, and $x \in \{1, 2, 3\}$. Moreover, $\mathbf{P}_1 = \mathbf{H}_1\mathbf{G}_1$, $\mathbf{P}_2 = \mathbf{H}_2\mathbf{G}_2$, and $\mathbf{P}_3 = \mathbf{H}_2\mathbf{T}\mathbf{G}_1$. We design the training matrices at the RISs, i.e., $\mathbf{\Theta}_1^0$, and $\mathbf{\Theta}_2^0$ as truncated DFT matrices. In all the simulations, we assume that $M_{\text{BS}} = 4$, $M_{\text{UE}} = 2$, $K = 2$, $M_{\text{S1}} = 30$, and $M_{\text{S2}} = 20$.

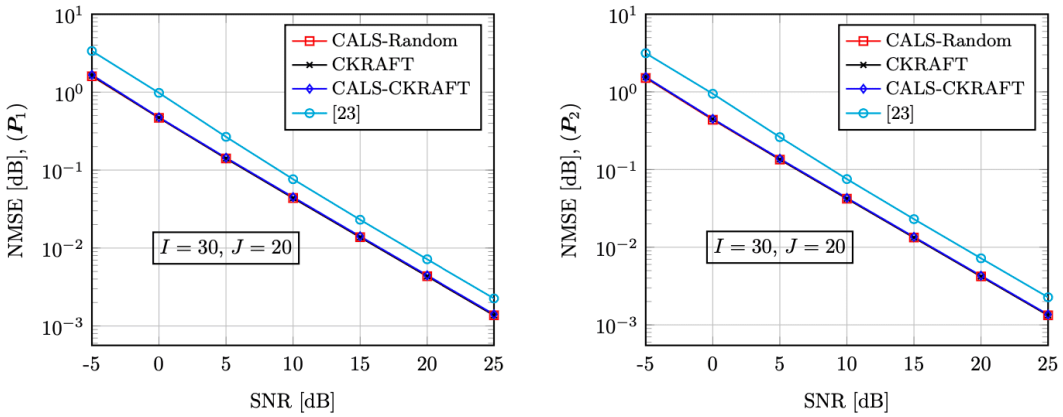

(a) NMSE vs SNR for $\boldsymbol{P}_1$ (b) NMSE vs SNR for $\boldsymbol{P}_2$

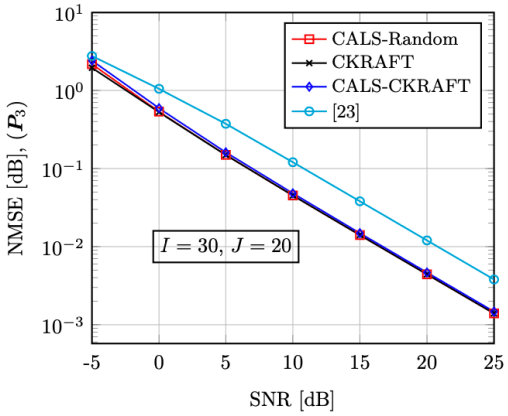

(c) NMSE vs SNR for $\boldsymbol{P}_3$

Figure 8. NMSE vs SNR of the cascaded channels, $M_{\text{S1}} = 30$, $M_{\text{S2}} = 20$, $\{I, J\} = \{30, 20\}$

In Figures 8(a) - 8(c), we show the NMSE versus the signal-to-noise ratio (SNR) for the cascaded channels in components 1, 2, and 3, respectively, comparing the two proposed channel estimation methods, the CKRAFT method, i.e., Algorithm 1,

the C-ALS method, i.e., Algorithm 2, and the channel estimation method in [23]. From the figures, we can see clearly that when I and J are selected such that $I = M_{S1}$ and $J = M_{S2}$, the proposed coupled tensor-based channel estimation frameworks, i.e., CKRAFT, Algorithm 2 with CKRAFT initialization and Algorithm 2 with random initialization have a better performance in comparison with the scheme in [23]. This performance improvement is as a result of the adopted coupled tensor decompositions which brought about significant gain in terms of the identifiablity constraints. The results show that C-KRAFT and C-ALS with random initialization have a similar performance. This implies that we do not have to use the C-ALS algorithm if the identifiability conditions for the C-KRAFT algorithm are satisfied. This is due to the fact that the C-ALS algorithm is computationally more expensive.

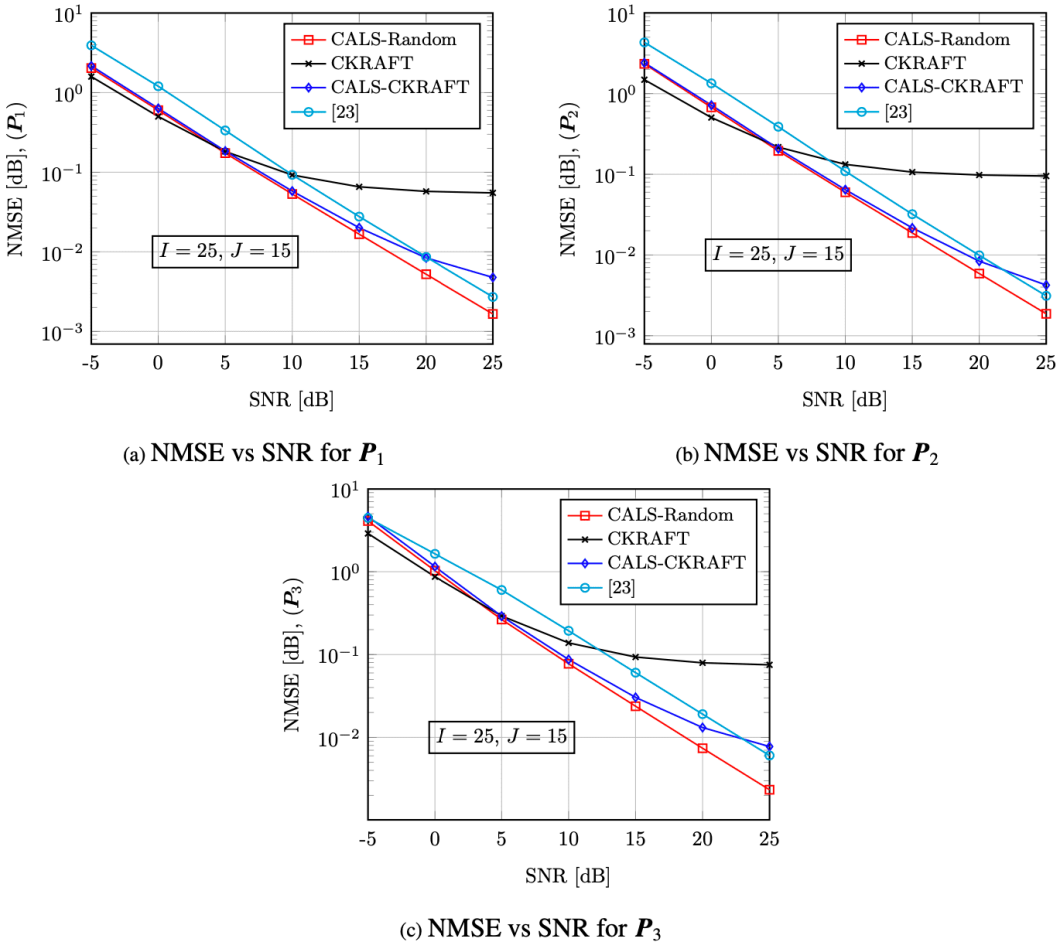

(a) NMSE vs SNR for $\boldsymbol{P}_1$

(b) NMSE vs SNR for $\boldsymbol{P}_2$

(c) NMSE vs SNR for $\boldsymbol{P}_3$

Figure 9. NMSE vs SNR of the cascaded channels, $M_{S1} = 30, M_{S2} = 20, \{I, J\} = \{25, 15\}$

In Figures 9(a) - 9(c), we show the NMSE versus the SNR for the cascaded channels in components 1, 2, and 3, respectively, while selecting $I < M_{S1}$ and $J < M_{S2}$. From the figures, we see that the performance of the CKRAFT algorithm degrades significantly. This performance degradation is due to the fact that the identifiability constraints for the CKRAFT algorithm given in Section 3.2.1 are not satisfied. However, the CALS algorithm with random initialization which is less restrictive in

doi.org/10.32388/V5XHXK

terms of the identifiability condition achieves a good performance at the expense of a higher complexity in terms of the number of iterations. The CALS algorithm attains agood performance only after a few iterations, i.e., $t_{\max} = 10$.

5. Conclusions

In this paper, we consider the channel estimation problem in D-RIS-aided flat-fading MIMO systems. To reduce the signaling overhead, we propose an interference-free channel training protocol, which allows us to extract the signal measurements of a particular reflection link interference-free from measurements of the superposition of the three links. To further improve the identifiability constraints and improve the channel estimation accuracy, we exploit the structure of the common channels and the inherent benefits of coupled tensor decompositions. We propose a closed-form solution based on the least square Khatrio-Rao factorization and an enhanced iterative solution using an alternating least square approach. Using the coupled tensor-based least square Khatri-Rao factorization (C-KRAFT) and the coupled-ALS (C-ALS) based channel estimation schemes, the channel matrices in both single and double reflection links are obtained. The C-ALS algorithm is less restrictive in terms of the identifiability condition at the expense of additional complexity with respect to the number of iterations. The results show that C-KRAFT and C-ALS with random initialization have a similar performance. This implies that we do not have to use the C-ALS algorithm if the identifiability conditions for the C-KRAFT algorithm are satisfied. The provided simulation results show the effectiveness of the proposed channel training protocol.

Appendix A. Detailed Derivation of (29)

To begin, we note the following identities, Property 1: $\text{vec}\{\mathbf{XYZ}\} = (\mathbf{Z}^{\mathsf{T}} \otimes \mathbf{X})\text{vec}\{\mathbf{Y}\}$. Property 2: $\text{vec}\{\mathbf{X}\text{diag}\{\mathbf{y}\}\mathbf{Z}\} = (\mathbf{Z}^{\mathsf{T}} \diamond \mathbf{X})\mathbf{y}$. Property 3: $\begin{bmatrix} \mathbf{A} \diamond \mathbf{C} \\ \mathbf{A} \diamond \mathbf{B} \end{bmatrix} = \mathbf{P}\left(\mathbf{A} \diamond \begin{bmatrix} \mathbf{C} \\ \mathbf{B} \end{bmatrix}\right)$, where $\mathbf{P}$ is a permutation matrix. Property 4: $\begin{bmatrix} \mathbf{A} \\ \mathbf{B} \end{bmatrix}^{\mathsf{T}} = \begin{bmatrix} \mathbf{A}^{\mathsf{T}} & \mathbf{B}^{\mathsf{T}} \end{bmatrix}$. Then, the coupled measurement matrix in (28) which is given as

$$\tilde{\mathbf{Y}}_1 = \mathbf{G}_1^{\mathsf{T}} \begin{bmatrix} \left(\mathbf{Q}_1 \diamond \mathbf{\Theta}_1^0 \diamond \mathbf{H}_1\right)^{\mathsf{T}} & \left(\mathbf{\Theta}_1^0 \diamond [\mathcal{U}]_{(3)}^{\mathsf{T}}\right)^{\mathsf{T}} \end{bmatrix}, \tag{A.1}$$

can be expressed as

$$\begin{aligned} \tilde{\mathbf{Y}}_1 &= \begin{bmatrix} \left\{\left(\mathbf{\Theta}_1^0 \diamond \mathbf{H}_1\right)\mathbf{G}_1\right\}^{\mathsf{T}} & \left\{\left(\mathbf{\Theta}_1^0 \diamond [\mathcal{U}]_{(3)}^{\mathsf{T}}\right)\mathbf{G}_1\right\}^{\mathsf{T}} \end{bmatrix} \\ &\overset{(a)}{=} \begin{bmatrix} \left\{\left(\mathbf{\Theta}_1^0 \diamond \mathbf{H}_1\right)\mathbf{G}_1\right\} \\ \left\{\left(\mathbf{\Theta}_1^0 \diamond [\mathcal{U}]_{(3)}^{\mathsf{T}}\right)\mathbf{G}_1\right\} \end{bmatrix}^{\mathsf{T}} \\ &\overset{(b)}{=} \left[\mathbf{P}\left[\mathbf{\Theta}_1^0 \diamond \underbrace{\begin{bmatrix} \mathbf{H}_1 \\ [\mathcal{U}]_{(3)}^{\mathsf{T}} \end{bmatrix}}_{\mathbf{\Sigma}_1}\right]\mathbf{G}_1\right]^{\mathsf{T}} = \left\{\mathbf{P}\left[\mathbf{\Theta}_1^0 \diamond \mathbf{\Sigma}_1\right]\mathbf{G}_1\right\}^{\mathsf{T}} = \mathbf{G}_1^{\mathsf{T}}\left[\mathbf{\Theta}_1^0 \diamond \mathbf{\Sigma}_1\right]^{\mathsf{T}}\mathbf{P}^{\mathsf{T}}, \end{aligned} \tag{A.2}$$

where (a) is due to the application of Property 4, (b) is obtained by using Property 4, and $\mathbf{P}$ is a permutation matrix.

References

1. ^Di Renzo M, Zappone A, Debbah M, Alouini M, Yuen C, de Rosny J, Tretyakov S (2020). "Smart radio environments empowered by reconfigurable intelligent surfaces: How it works, state of research, and the road ahead." IEEE Journal on Selected Areas in Communications. 38 (11): 2450–2525. doi:10.1109/JSAC.2020.3007211.

2. ^Liaskos C, Nie S, Tsioliaridou A, Pitsillides A, Ioannidis S, Akyildiz I (2018). "A new wireless communication paradigm throug h software-controlled metasurfaces." IEEE Communications Magazine. **56** (9): 162–169. doi:10.1109/MCOM.2018.1700659.
3. a, bCao Y, Lv T, Lin Z, Ni W (2021). "Delay-constrained joint power control, user detection and passive beamforming in intelli gent reflecting surface-assisted uplink mmwave system." IEEE Transactions on Cognitive Communications and Networking. **7** (2): 482–495. doi:10.1109/TCCN.2021.3064973.
4. a, bNwalozie GC, Ardah K, Haardt M. Reflection design methods for reconfigurable intelligent surfaces-aided dynamic TDD sy stems. In: Proceedings of IEEE 12th Sensor Array and Multichannel Signal Processing Workshop (SAM 2022); June 2022. http s://doi.org/10.1109/SAM53842.2022.9827850
5. a, bNwalozie GC, Haardt M. Distributed coordinated beamforming for RIS-aided dynamic TDD systems. In: Proceedings of 26t h International ITG Workshop on Smart Antennas and 13th Conference on Systems, Communications, and Coding (WSA and S CC 2023); February 2023; Braunschweig, Germany. https://ieeexplore.ieee.org/xpl/conhome/10104032/proceeding
6. a, bYuan J, Liang Y, Joung J, Feng G, Larsson EG. Intelligent reflecting surface-assisted cognitive radio system. IEEE Trans Com mun. 2021;69(1):675-87. https://doi.org/10.1109/TCOMM.2020.3033006
7. a, bPogaku AC, Do D, Lee BM, Nguyen ND (2022). "UAV-assisted RIS for future wireless communications: A survey on optimiz ation and performance analysis." IEEE Access. **10**: 16320–16336. doi:10.1109/ACCESS.2022.3149054.
8. a, bNadeem Q, Alwazani H, Kammoun A, Chaaban A, Debbah M, Alouini M (2020). "Intelligent reflecting surface-assisted mu lti-user MISO communication: Channel estimation and beamforming design." IEEE Open Journal of the Communications Soci ety. **1**: 661–680. doi:10.1109/OJCOMS.2020.2992791.
9. ^Nwalozie GC, Haardt M. "Leakage-based Coordinated Beamforming for RIS-aided Dynamic TDD Systems." In: Proc. of 31st European Signal Processing Conference (EUSIPCO 2023), Helsinki, Finland, September 2023. doi:10.23919/EUSIPCO58844.20 23.10289836.
10. a, b, c, dde Araújo GT, de Almeida ALF, Boyer R (2021). "Channel estimation for intelligent reflecting surface assisted MIMO sy stems: A tensor modeling approach." IEEE Journal of Selected Topics in Signal Processing. **15** (3): 789–802. doi:10.1109/JSTSP. 2021.3061274.
11. ^Gherekhloo S, Ardah K, de Almeida ALF, Haardt M. "Tensor-based channel estimation and reflection design for RIS-aided m illimeter-wave MIMO communication systems." In: Proc. of 55th Asilomar Conference on Signals, Systems, and Computers; 2 021. p. 1683–1689. doi:10.1109/IEEECONF53345.2021.9723362.
12. ^Zheng B, You C, Zhang R (2021). "Double-IRS assisted multi-user MIMO: Cooperative passive beamforming design." IEEE Tr ansactions on Wireless Communications. **20** (7): 4513–4526. doi:10.1109/TWC.2021.3059945.
13. ^Bazzi S, Xu W. IRS parameter optimization for channel estimation MSE minimization in double-IRS aided systems. IEEE Wir el Commun Lett. 2022;11(10):2170-4. https://doi.org/10.1109/LWC.2022.3196126
14. ^You C, Zheng B, Zhang R. "Wireless communication via Double IRS: Channel estimation and passive beamforming designs." IEEE Wireless Communications Letters. **10** (2): 431–435, 2021. doi:10.1109/LWC.2020.3034388.
15. ^Le HA, Chien TV, Nguyen VD, Choi W (2023). "Double RIS-assisted MIMO systems over spatially correlated Rician fading cha nnels and finite scatterers." IEEE Transactions on Communications. **71** (8): 4941–4956. doi:10.1109/TCOMM.2023.3280209.
16. ^Han Y, Zhang S, Duan L, Zhang R (2020). "Cooperative Double-IRS aided communication: Beamforming design and power scaling." IEEE Wireless Communications Letters. **9** (8): 1206–1210. doi:10.1109/LWC.2020.2986290.

17. ^ a b c *Ardah K, Gherekhloo S, de Almeida ALF, Haardt M. "Double-RIS versus Single-RIS aided systems: Tensor-based MIMO c hannel estimation and design perspectives." In: Proceedings of IEEE International Conference on Acoustics, Speech and Signal Processing (ICASSP); 2022. p. 5183–5187. doi:10.1109/ICASSP43922.2022.9746287.*

18. ^ a b c d e *Gherekhloo S, Ardah K, de Almeida ALF, Maleki M, Haardt M. "Nested PARAFAC tensor-based channel estimation m ethod for double RIS-aided MIMO communication systems." In: Proc. of European Signal Processing Conference (EUSIPCO); 2 023. doi:10.23919/EUSIPCO58844.2023.10290107.*

19. ^ *Zheng B, You C, Zhang R (2021). "Efficient channel estimation for Double-IRS aided multi-user MIMO system." IEEE Transa ctions on Communications. **69** (6): 3818–3832. doi:10.1109/TCOMM.2021.3064947.*

20. ^ a b *Yang S, Lyu W, Xiu Y, Zhang Z, Yuen C (2023). "Active 3D Double-RIS-aided multi-user communications: Two-timescale- based separate channel estimation via Bayesian learning." IEEE Transactions on Communications. **71** (6): 3605–3620. doi:10. 1109/TCOMM.2023.3265115.*

21. ^ a b c d *Zheng B, You C, Zhang R. "Uplink channel estimation for Double-IRS assisted multi-user MIMO." In: Proc. of IEEE Inte rnational Conference on Communications (ICC); 2021. p. 1–6. doi:10.1109/ICC42927.2021.9501057.*

22. ^ *Liu M, Li X, Ning B, Huang C, Sun S, Yuen C (2023). "Deep learning-based channel estimation for Double-RIS aided massive MIMO system." IEEE Wireless Communications Letters. **12** (1): 70–74. doi:10.1109/LWC.2022.3217294.*

23. ^ a b c d e f g h i j *Gherekhloo S, Ardah K, Nwalozie GC, de Almeida ALF, Haardt M. "An efficient channel training protocol for channel estimation in double RIS-aided MIMO systems." In: Proc. of 32nd European Signal Processing Conference (EUSIPCO 2024), Lyon, France, August 2024. doi:10.23919/EUSIPCO63174.2024.10715192.*

24. ^ a b *de Almeida ALF, Favier G (2013). "Double Khatri–Rao space-time-frequency coding using semi-blind PARAFAC-based re ceiver." IEEE Signal Processing Letters. **20** (5): 471–474. doi:10.1109/LSP.2013.2248149.*

25. ^ *Chen J, Liang YC, Cheng HV, Yu W (2023). "Channel Estimation for Reconfigurable Intelligent Surface Aided Multi-User mm Wave MIMO Systems". IEEE Transactions on Wireless Communications. **22** (10): 6853–6869. doi:10.1109/TWC.2023.3246264.*

26. ^ *Ximenes LR, Favier G, de Almeida ALF (2015). "Semi-blind receivers for non-regenerative cooperative MIMO communicatio ns based on nested PARAFAC modeling." IEEE Transactions on Signal Processing. **63** (18): 4985–4998. doi:10.1109/TSP.2015. 2454473.*

27. ^ *Roemer F, Schroeter C, Haardt M. "A semi-algebraic framework for approximate CP decompositions via joint matrix diagon alization and generalized unfoldings." In: Proc. of the Forty Sixth Asilomar Conference on Signals, Systems and Computers; 20 12. p. 2023–2027.*

28. ^ *Roemer F, Haardt M (2010). "Tensor-based channel estimation (TENCE) for two-way relaying with multiple antennas and spatial reuse." IEEE Transactions on Signal Processing. **58** (11): 5720–5735. doi:10.1109/TSP.2010.2062179.*

29. ^ a b c *Ximenes LR, Favier G, de Almeida ALF (2016). "Closed-form semi-blind receiver for MIMO relay systems using double K hatri–Rao space-time coding." IEEE Signal Processing Letters. **23** (3): 316–320. doi:10.1109/LSP.2016.2518699.*

30. ^ *de Araujo GT, de Almeida ALF. "PARAFAC-based channel estimation for intelligent reflective surface assisted MIMO syste m." In: Proc. of 2020 IEEE 11th Sensor Array and Multichannel Signal Processing Workshop (SAM). 2020. p. 1–5. doi:10.1109/S AM48682.2020.9104260.*

31. ^ *Comon P, Luciani X, de Almeida ALF. "Tensor decompositions, alternating least squares and other tales." Journal of Chemo metrics. **23** (7-8): 393–405. doi:10.1002/cem.1236.*

Declarations

Funding: No specific funding was received for this work.

Potential competing interests: No potential competing interests to declare.